Self-Assembly of Silk-Collagen-like Triblock Copolymers Resembles a Supramolecular Living Polymerization

Lennart H. Beun,[†,*] Xavier J. Beaudoux,[†] J. Mieke Kleijn,[†] Frits A. de Wolf,[‡] and Martien A. Cohen Stuart[†]

[†]Laboratory of Physical Chemistry and Colloid Science, Wageningen University, Dreijenplein 6, 6703 HB, Wageningen, The Netherlands and [‡]Wageningen UR Food & Biobased Research, Bornse Weilanden 9, NL-6708 WG Wageningen, The Netherlands

ABSTRACT

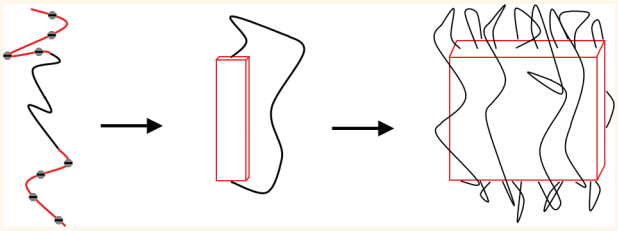

We produced several pH-responsive silk-collagen-like triblocks, one acidic and two alkaline. At pH values where the silk-like block is uncharged the triblocks self-assemble into filaments. The pH-induced self-assembly was examined by atomic force microscopy, light scattering, and circular dichroism. The populations of filaments were found to be very monodisperse, indicating that the filaments start to grow from already present nuclei in the sample. The growth then follows pseudo-first-order kinetics for all examined triblocks. When normalized to the initial concentration, the growth curves of each type of triblock overlap, showing that the self-assembly is a generic process for silk-collagen-silk triblocks, regardless of the nature of their chargeable groups. The elongation speed of the filaments is slow, due to the presence of repulsive collagen-like blocks and the limited number of possibilities for an approaching triblock to successfully attach to a growing end. The formation of filaments is fully reversible. Already present filaments can start growing again by addition of new triblocks. The structure of all filaments is very rich in β-turns, leading to β-rolls. The triblocks attain this structure only when attaching to a growing filament.

KEYWORDS: pH-responsive · biopolymer · protein · hydrogel · kinetics

Filamentous protein structures are widely studied and are important in many fields of research. They are crucial for several biological functions,[1,2] play an important role in certain diseases,[3,4] and have a major influence on food structures.[5−7] Understanding the process of filament formation is essential to be able to control their final size and shape and therefore their function. We developed a new class of stimulus-responsive biopolymers that can self-assemble into filamentous structures. These biologically synthesized protein polymers form a monodisperse system with an exactly defined length and sequence, stored in one genetic template. These properties are superior to those achieved with any established chemical polymerization method.

In this article we present our experimental work on the self-assembly behavior of silk-collagen-like triblock copolymers into filamentous structures. These triblocks consist of a hydrophilic and inert collagen-based part (C), which is 198 amino acids long and is very rich in glutamine, arginine, and serine, and a silk-based part (S) that consists of 24 octapeptide repeats (GAGAGAGX). We use three different silk blocks, where the X position in the glycine- and alanine-rich octapeptide is taken by either glutamic acid (E), histidine (H), or lysine (K). This way we have three different silk blocks that are all pH-responsive, of which one is acidic (S^E) and two are alkaline (S^H and S^K). We produced triblocks in two different arrangements, either with the collagen blocks on the outside and two silk blocks on the inside (CSSC) or with the silk blocks on the outside and two collagen blocks on the inside (SCCS). Together with the three variants in silk blocks, this gives us six different proteins. This study shows experimental results on the three silk-collagen-silk triblock proteins, indicated in Table 1.

Previous work showed that the histidine-bearing triblocks (CS^HS^HC and S^HCCS^H) self-assemble upon increasing the pH to a value higher than the pK of histidine.[8] The glutamic acid-bearing triblock shows similar behavior at a pH below the pK of the side group. The self-assembled triblocks have a filamentous structure with stacked β-rolls made up of the uncharged silk block and a dilute hydrophilic corona (loop) of the collagen-like block.[8] These β-rolls are composed of

* Address correspondence to Lennart.Beun@wur.nl.

Received for review August 12, 2011 and accepted December 14, 2011.

Published online December 14, 2011
10.1021/nn203092u

© 2011 American Chemical Society

TABLE 1. Overview of Different Triblocks Described in This Research

	acidic	alkaline	alkaline
silk-collagen-silk	S^ECCS^E	S^HCCS^H	S^KCCS^K
p*K*	~4.1	~6.5	~10

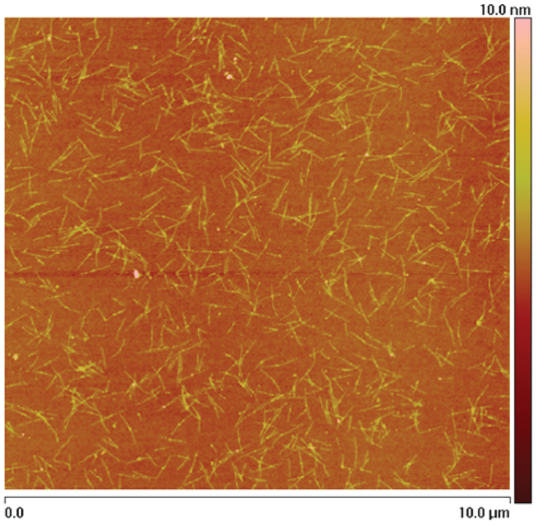

Figure 1. AFM tapping mode image of S^ECCS^E triblock filaments formed at pH 2.3 and adsorbed on a silica surface.

two parallel β-sheets, oriented in opposite directions and connected *via* β-turns. This way hydrogen bonds can be formed within each parallel β-sheet and between the oppositely oriented β-sheets. The β-rolls differ from the antiparallel β-sheets that are formed when crystallizing the silk domains in methanol.[9] The combination of a silk-like domain and a collagen-like one can yield interesting properties. These bioinspired triblock copolymers make use of the unique combination of flexibility and strength of silk[9−14] and the excellent biocompatibility of collagen, which has been widely studied as a basis for tissue engineering.[15−18]

In this work we elucidate the self-assembly kinetics of three different silk-collagen-like triblock copolymers. Using microscopy, light scattering, and circular dichroism we investigate the formation of supramolecular filaments after charge neutralization. We use both acidic and alkaline triblocks to study the self-assembly of the neutralized polymer under different pH conditions. We look at the concentration dependence of the self-assembly process and at the structure of the different triblocks in the self-assembled state. Furthermore, we look into the reversibility of the pH-induced self-assembly.

RESULTS AND DISCUSSION

Atomic Force Microscopy. Samples that contained filaments after self-assembly of individual triblocks were analyzed by tapping mode AFM. An example can be seen in Figure 1. Interestingly, the filaments visible in this image have a remarkably narrow length distribution.

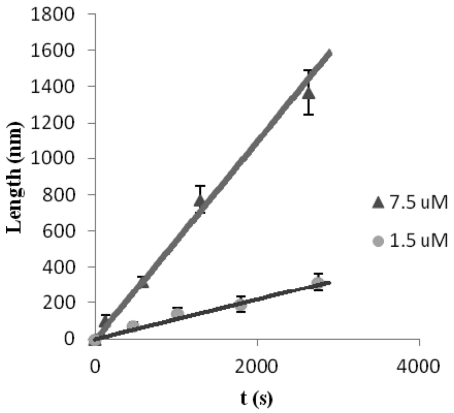

Figure 2. Elongation of growing filaments of S^ECCS^E measured with AFM tapping mode for different triblock concentrations. Error bars represent standard deviations of 10 measured filaments per time step. The lines represent calculated values according to eq 4.

TABLE 2. Initial Filament Elongation Speed of S^ECCS^E Triblock at pH 2.3

triblock concentration	elongation speed
1.5 μM	0.11 nm/s
7.5 μM	0.58 nm/s

For different times after the start of the self-assembly, we imaged the adsorbed and dried filaments and measured their contour length. Results are shown in Figure 2. As can be seen, in the initial phase the length increases linearly in time; from the slope a value for the elongation speed of the growing filaments can be obtained (Table 2).

The presence of a very monodisperse system of filaments at all times shows that an initial fast nucleation step is followed by elongation by the attachment of new triblocks. This experiment shows that the individual filaments have a growth speed that has a first-order dependency on the triblock concentration $c(t)$.

$$\frac{dL}{dt} = k_a c(t) \qquad (1)$$

From Figure 2, the value of the rate constant k_a can be determined as being 7.7×10^{-8} m^4 mol^{-1} s^{-1}.

The monodisperse population of filaments, which is visible in Figure 2, suggests a nucleated growth mechanism with a fixed number of initial nuclei n (mol m^{-3}). The same is found for the two alkaline triblocks that were examined. These nuclei can be impurities that were not removed during the purification or partially digested triblocks. As for a certain triblock, per batch, the length of the filaments that are visible on AFM pictures after completion of the self-assembly does not depend on concentration, we conclude that the ratio

of the concentration of nuclei (n) to the initial concentration of triblock is a constant. This aggregation number N also corresponds to the average number of triblock molecules in one filament after completion of the self-assembly:

$$N = \frac{c(0)}{n} \tag{2}$$

The concentration of free triblocks that determines the growth speed of the filaments can be expressed as a function of the total concentration of protein $c(0)$ and the concentration of proteins in the filaments.

$$c(t) = c(0) - \frac{c(0)}{Nl} L(t) \tag{3}$$

with $n = c(0)/N$ the concentration, $L(t)$ the contour length of the filaments, and l the length per molecule of triblock in the filament.

Substituting this equation for $c(t)$ in eq 1 gives us a differential equation that can be solved into

$$L(t) = \frac{c(0)l}{n}\left[1 - \exp\left(-k_a \frac{c(0)}{Nl} t\right)\right] \tag{4}$$

This equation gives an excellent match with the measured data presented in Figure 2.

If we compare the elongation speed of the growing filaments with the flocculation of Brownian particles according to Smoluchowski, we can compare the elongation speed with that of a diffusion-limited case. The Smoluchowski equation for our case gives the decrease of the concentration of triblocks dc/dt as a function of the concentration of the triblocks c, the concentration of filaments n, Avogadro's number N_A, and the kinetic parameter K_{Brown}.

$$-\frac{dc}{dt} = K_{Brown} c n N_A \tag{5}$$

The parameter K_{Brown} is a function of the absolute temperature T, the viscosity of the solution η, and Boltzmann constant k_b:

$$K_{Brown} = \frac{4k_b T}{3\eta} \tag{6}$$

We can express dc/dt in terms of the elongation speed dL/dt, the concentration of filaments n, and the length per triblock molecule in the filament l.

$$-\frac{dc}{dt} = \frac{dL}{dt}\frac{n}{l} \tag{7}$$

Combining these equations gives a value for dL/dt:

$$\frac{dL}{dt} = K_{Brown} c l N_A \tag{8}$$

For the solution of S^ECCS^E of 1.5 μM and a value for l of 0.95 nm[19] this leads to a value for dL/dt of 4.6 μm/s, which is more than 4 orders of magnitude higher than experimentally found and shown in Table 2. We have several explanations for this difference. First of all the Smoluchowski equation does not account for the limited part of the growing filament that is available for aggregation. Only a collision between a growing end of a filament and a free triblock can lead to the elongation of that filament. Furthermore, the steric nature of the glutamic acid leads to a lower number of successful collisions. There must be a parallel stacking of the triblocks in order for the glutamic acid groups not to overlap.[19−21] As a consequence, the conformation and orientation of the triblocks when approaching a growing end is essential for attachment to the filament. An unfavorable conformation will thus not lead to the attachment of the new triblock. Finally, the good solubility of the collagen part induces a repulsive interaction between the filament and the approaching triblock that leads to an energy barrier to be overcome. This energy barrier also leads to a lower success rate of elongation per collision.

Static Light Scattering. According to the Rayleigh theory, the light scattered by a solution is given by the sum of the scattered intensity of all particles in solution. The light scattered is usually given as the Rayleigh ratio R and can be written as the sum of the scattering by the individual particles in solution:

$$R = K \sum_i c_i M_i^2 P_i(q) S(q) \tag{9}$$

where c is the concentration, M the molar mass, $P(q)$ the form factor that accounts for interference of scattered light within one particle, and $S(q)$ the structure factor that accounts for interference of scattered light from different particles in the solution. The optical constant K is given by

$$K = 4\pi^2 n_0^2 \left(\frac{dn}{dc}\right)^2 / N_A \lambda^4 \tag{10}$$

where n_0 is the refractive index of the solvent, dn/dc is the refractive index increment of the solute (0.18 cm^3/g for our triblocks), N_A is Avogadro's number, and λ is the wavelength of the light *in vacuo*.

The Rayleigh ratio R can be determined by measuring the scattered intensity of a sample, the pure solvent, and a reference sample of which the Rayleigh ratio is known:

$$R_{sam} = \frac{I_{sam} - I_{sol}}{I_{ref}} \times R_{ref} \times \frac{n_{sam}^2}{n_{ref}^2} \tag{11}$$

As a reference, toluene was taken, which has a known Rayleigh ratio of 1.98 $\times$ 10^{-5} cm^{-1} at the used wavelength.[22]

Figure 3 shows the development of R/c for a solution of S^ECCS^E after decreasing the pH to 2.3.

We see that, directly after acidification of the sample, there is a steady increase of the scattered light intensity, showing that the size of the particles in solution is increasing continuously. From the rate of

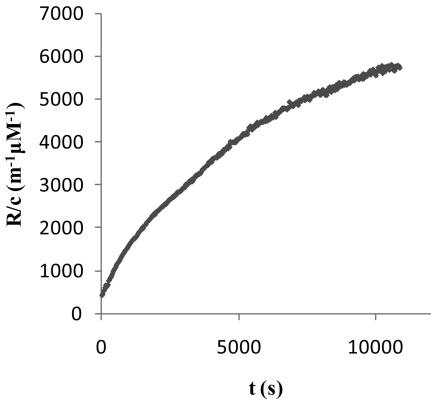

Figure 3. Static light scattering data of a 1.5 μM S^ECCS^E solution at pH 2.3.

increase we can obtain information about the kinetics of the self-assembly process.

For a monodisperse population of linear particles in a dilute solution as in our study, we can assume $S(q) = 1$, and eq 9 can be rewritten as

$$R = Kn\frac{M_w^2 L^2}{I^2}P(qL) \quad (12)$$

with n being the filament concentration, M_w the molar mass of the individual triblock, I the length per triblock in the filament, and L the contour length of the scattering particles.

Combining eqs 4 and 12 gives an expression for $R(t)$ for a monodisperse population of growing filaments:

$$R(t) = \frac{KM_w^2 c(0)^2}{n}\left[1 - \exp\left(-k_a\frac{c(0)}{NI}t\right)\right]^2 P(qL) \quad (13)$$

Rewriting this equation shows that for a system that displays pseudo-first-order kinetics, plotting $R/c(0)$ against $c(0)t$ for different concentrations of triblock gives graphs that will overlap if the shape of the filaments and thus the form factor $P(qL)$ develops in the same way. Equation 4 shows that the length of the filaments $L(t)$ is a function of the combined variable $c(0)t$. The wavevector q is constant, which means that the form factor $P(qL)$ is also a function of $c(0)t$. Dividing eq 13 by $c(0)$ leads to the expression below that contains the values K, N, I, and k_a, which are all constants for a given triblock. The only variables in the equation are $c(0)$, t, and $P(qL)$.

$$\frac{R(t)}{c(0)} = KM_w^2 N\left[1 - \exp\left(\frac{-k_a c(0)t}{NI}\right)\right]^2 P(qL) \quad (14)$$

From the AFM pictures it is clear that the shape of the filaments does not depend on the concentration of triblock in a sample. The development of the form factor $P(qL)$ depends only on $L(t)$, which according to eq 4 scales with $c(0)t$. Figure 4 shows plots in which the Rayleigh ratio per concentration of triblock $R/c(0)$ is plotted against $c(0)t$.

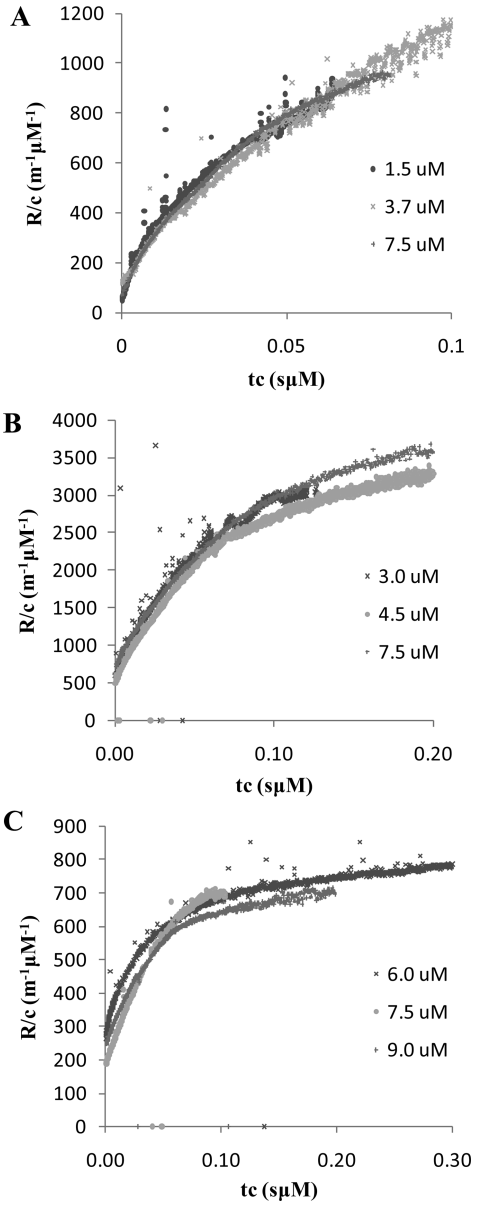

Figure 4. Static light scattering data for self-assembly of different triblocks. (A) S^ECCS^E triblock solutions of different concentrations at pH 2.3. (B) S^HCCS^H triblock solutions of different concentrations at pH 11. (C) S^KCCS^K triblock solutions of different concentrations at pH 12.

Figure 4 shows that indeed for every separate triblock plots of $R/c(0)$ against $c(0)t$ for different concentrations overlap. This confirms our hypothesis that the self-assembly process follows pseudo-first-order kinetics. It also shows that this behavior is generic for silk-collagen-silk triblocks, regardless of the nature of the chargeable group.

After completion of the self-assembly process it is possible to restart the growth of the filaments by adding a fresh solution of triblocks, similar to that in a living polymerization process.[23] This is shown in Figure 5 for a solution of 7.5 μM S^ECCS^E at pH 2.3. The first part of the plot shows an increase in Rayleigh ratio by the self-assembly of individual triblocks into

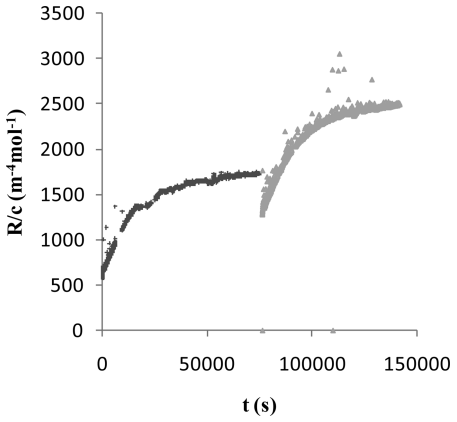

Figure 5. Static light scattering data for the self-assembly of a 7.5 μM solution of S^ECCS^E at pH 2.3. At t = 75 000 s half of the solution was removed and a fresh solution of free S^ECCS^E triblocks and acid was added to reach the same concentration, volume, and pH as before.

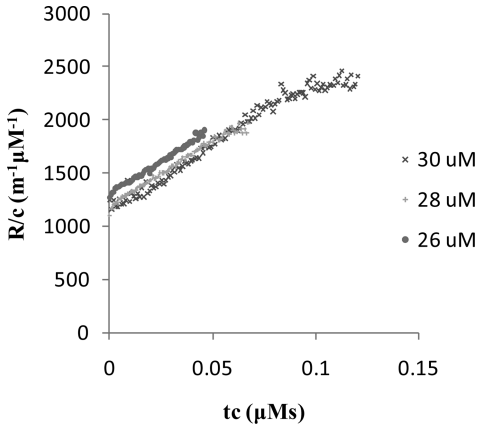

Figure 7. Static light scattering data for S^ECCS^E directly after lowering the pH to 2.3 (30 μM). The two other graphs show data obtained after increasing the pH to 10 again and acidifying to pH 2.3 a second time (28 μM), and repeating this procedure once more (26 μM).

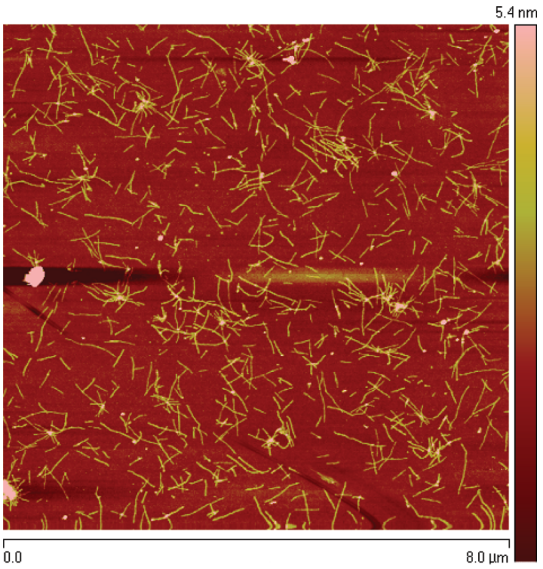

Figure 6. AFM tapping mode image of a bidisperse population of filaments formed in a 7.5 μM solution of S^ECCS^E at pH 2.3. The two populations have an average length for 20 filaments each of 320 $\pm$ 43 and 850 $\pm$ 67 nm.

filaments. The solution was left until the scattered light intensity was stable and all triblocks were present in filaments. Then half of the solution was removed, and fresh triblock and acid was added to obtain the same concentration and pH. As expected, this resulted in a Rayleigh ratio that is exactly the average of that of both solutions. The Rayleigh ratio immediately starts to increase again, indicating that self-assembly has started again. The final value of the Rayleigh ratio is higher than the first plateau value. Therefore, we conclude that the already present filaments start growing again once new triblock is added to the solution. If only new filaments would be formed, the second plateau would be the same as the first, as a monodisperse population of filaments of size L would be formed. Due to the quadratic dependence of the scattered intensity on particle size, the bidisperse population that consists half of filaments of size $L - x$ and half of filaments of size $L + x$ has a higher total scattered intensity, as shown in Figure 5.

In addition we see that an AFM image taken at the end of this experiment shows a bidisperse population of filaments. This image is presented in Figure 6. This supports our light-scattering data that the present filaments start growing again and that new filaments are formed when fresh solution is added.

When the pH of a solution with filaments is changed to a value well above the pK for the acidic triblock or below the pK for the alkaline triblocks, we observe an instant drop in scattered light intensity to a value that corresponds to the scattering of triblocks in their unassembled state. This indicates the breakup of filaments into individual charged triblocks. After this, self-assembly into filaments can be induced again by changing the pH to an appropriate value. In Figure 7 we show static light scattering data for a solution of S^ECCS^E that was acidified for a second time to a pH of 2.3 after breaking up the filaments by adding NaOH. Previous work shows that the critical pH at which these filaments break up is 5.4.[24]

In Figure 7 we see that again lowering the pH to 2.3 gives us the same development of the signal $R/c(0)$, after correction for the dilution by the extra added acid and base. Repeating this procedure again gives us a corresponding development of $R/c(0)$. These data show that the self-assembly of triblocks is a fully reversible process. It also confirms that the concentration of nuclei is proportional to the concentration of triblock in the sample. We attribute the small vertical shifts of the plots to the increase of salt due to the addition of acid and base.

Circular Dichroism. CD measurements were used to compare the secondary structure of the three triblocks

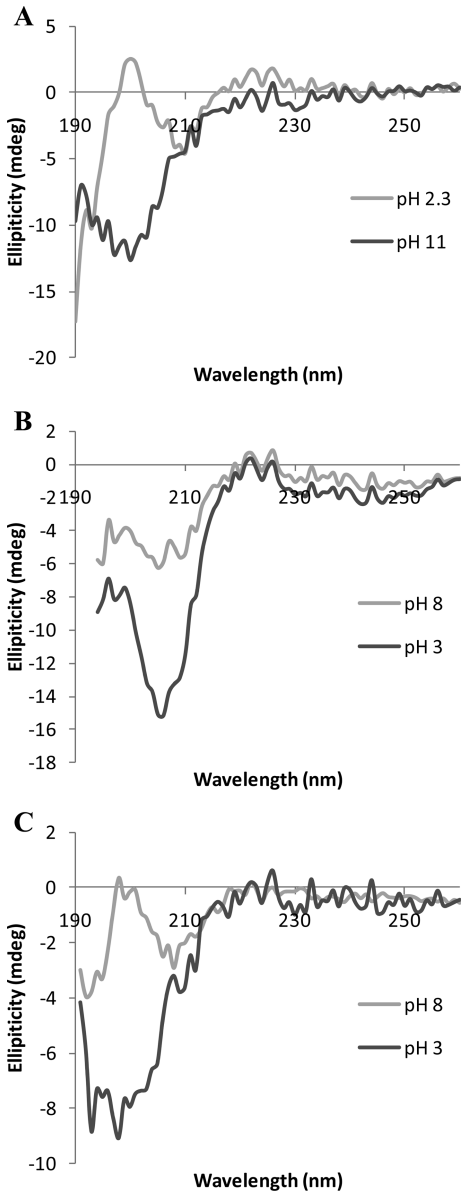

Figure 8. Circular dichroism spectra of three different triblocks in their charged colloidal state and after self-assembly into filaments. (A) A 1.5 μM solution of S^ECCS^E at pH 11 and 24 h after acidification to pH 2.3. (B) A 1.5 μM solution of S^HCCS^H at pH 3 and 24 h after changing the pH to 7.9. (C) A 4.5 μM solution of S^KCCS^K at pH 3 and 24 h after changing the pH to 12.

S^ECCS^E, S^HCCS^H, and S^KCCS^K. For each triblock we recorded a spectrum in the charged colloidal state and in the self-assembled state. We left the solutions for 24 h for the self-assembly to complete.

It has already been shown that glutamic acid-bearing triblocks are very rich in β-turns once filaments are formed.[8] These β-turns are present in so-called β-rolls, as demonstrated by molecular dynamics simulations. The data on S^KCCS^K presented in Figure 8 show a spectrum very similar to that of the other two triblocks. In the charged form (pH 3) it has a clear negative ellipticity around 197 nm. After the formation of

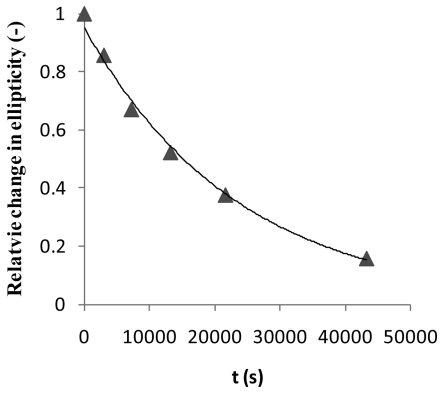

Figure 9. Relative change of the ellipticity at 197 nm of a 1.5 μM solution of S^ECCS^E during the self-assembly process at pH 2.3. The curve shows a monoexponential decay of the fraction of triblock in the unassembled state.

filaments this negative ellipticity almost disappears, very much like the spectrum of S^ECCS^E. The most significant difference is that the spectrum for S^KCCS^K is somewhat less pronounced, as we need a higher concentration to obtain the same ellipticity. The spectrum of S^HCCS^H looks like an intermediate form of the random coil spectrum and the β-roll structure. This can be a result of the bulky and hydrophobic nature of the histidine side chain. The bulky nature of the histidine side chain at the turn can disturb this structure and decrease its impact on the CD spectrum. The hydrophobic character of the uncharged histidine side chain can lead to the incorporation of improperly folded triblock molecules in the filament. These molecules are then kinetically trapped and do not contribute to the signal of the β-roll structure, but are visible as random coiled structures in the CD spectrum.

We measured the spectrum of a 1.5 μM solution of S^ECCS^E in time to determine the evolution of the secondary structure during the self-assembly into filaments. We observed no clear shift in the spectrum directly after lowering the pH to 2.3. The shift from random coil to β-roll structure is slow and occurs on the same time scale as the formation of the filaments. Therefore we conclude that the triblock attains the β-roll structure only when attaching to a growing end of a filament. In Figure 9 we plotted the relative change of the ellipticity θ at 197 nm, calculated as $[\theta(\infty) - \theta(t)]/[\theta(\infty) - \theta(0)]$. This ratio expresses the fraction of triblock that is still in the unassembled state.

The plot in Figure 9 shows a monoexponential decay of this fraction, which is consistent with pseudo-first-order kinetics. This supports our conclusion that a triblock attains a β-roll structure during self-assembly into filaments.

CONCLUSIONS

Silk-collagen-like triblock copolymers follow pseudo-first-order kinetics during self-assembly in dilute solutions. The slow growth in these dilute solutions

enabled us to follow the length development of populations of filaments in time. Using light scattering we could investigate the growth kinetics in a system without dealing with a steep increase in viscosity during gel formation. The formation of filaments after charge neutralization shows generic behavior for the acidic (S^ECCS^E) and alkaline (S^HCCS^H and S^KCCS^K) triblocks. Each triblock forms ribbonlike filaments when the pH is adjusted to a value at which the triblock is uncharged. The narrow length distribution of the population of filaments suggests a nucleated growth mechanism from already present nuclei in the sample. The consecutive elongation of the growing filaments shows a first-order concentration dependence. Elongation can be restarted by addition of new triblocks. The elongation speed is much slower than expected for a random aggregation mechanism. This is attributed to the repulsive nature of the collagen block, the limited size and availability of the growing end of a filament, and the orientation and conformation that is needed for an approaching triblock to successfully attach to a growing filament. Charging up the filaments by altering the pH creates a very unstable situation in which the filaments immediately fall apart into individual triblocks. The self-assembly into filaments can then be triggered again by altering the pH to a value at which the triblocks are uncharged. The kinetic properties of this repeated self-assembly, when corrected for dilution, are identical to those of the freshly prepared solution. Therefore, we conclude that the nuclei present in the sample stay intact and the pH-induced self-assembly is reversible. The structure of the filaments of all three types of triblocks is very rich in β-turns, forming β-rolls. Surprisingly, the formation of these β-rolls does not occur directly after neutralization, but only upon attachment to a filament, illustrated by the slow evolution of the CD spectrum from random coil to β-rolls. The kinetic properties of the self-assembly process are very similar to those of a living polymerization reaction, with the exception that the self-assembly is a reversible supramolecular process.

EXPERIMENTAL SECTION

Protein Sequence and Synthesis. The amino acid sequences of S^ECCS^E, CS^ES^EC, and S^HCCS^H have been described previously.[25] The S^KCCS^K triblock differs from the S^ECCS^E and S^HCCS^H triblocks only in the silk part, where the GAGAGAGX repeat bears a lysine (K) in the X position instead of glutamic acid (E) or histidine (H), respectively. All triblocks were produced in a fed batch fermentation of *Pichia pastoris* as previously described for the glutamic acid- and histidine-bearing triblocks. The S^KCCS^K was produced and purified in the same way as the S^HCCS^H triblock.

Static Light Scattering. Static light scattering data were all obtained at a 90° angle using an ALV-SP/86 goniometer with an ALV7002 external correlator and a Thorn RFIB263KF photomultiplier detector with 200/400 μm pinhole detection system. It was operated using a 300 mW Cobolt Samba-300 DPSS laser at a wavelength of 532 nm. The setup corresponds to a wavevector of 0.022 nm^{-1}. All samples were measured in round quartz cuvettes, including solvent blanks, for which water was used. As a reference sample we used toluene. Samples were prepared by mixing the appropriate amount of protein stock solution and demineralized water. After adding a 50 mM HCl or NaOH solution to reach a final concentration of 10 mM the sample was immediately shaken and filtered with a Nalgene 200 nm syringe filter. Subsequently the solution was transferred to the quartz cuvette and the measurement was started. The average time between the start of the experiment and the start of the measurement was 1 min. After the experiment had finished, we measured the pH of each sample.

AFM Imaging. AFM samples were made by dipping a 10×10 mm hydrophilic silicon wafer bearing a thin oxide layer into the protein solution, rinsing with demineralized water to remove any nonadsorbed material, and drying it under a stream of nitrogen. The samples were analyzed using a Digital Instruments Nanoscope III in tapping mode with NANOSENSORS SSS-NCH-20 silicon tips with a typical tip radius of 2 nm.

Circular Dichroism. CD measurements were performed on a Jasco J-715 spectropolarimeter at room temperature. The spectra were recorded between 190 and 260 nm with a resolution of 0.2 nm and a scanning speed of 1 nm/s. Spectra were recorded for three different triblocks: S^ECCS^E, S^HCCS^H, and S^KCCS^K. First spectra were recorded for each triblock in the unassembled state. For S^ECCS^E we used a 1.5 μM solution in 1 mM NaOH, for S^HCCS^H we used a 1.5 μM solution in 1 mM HCl, and for S^KCCS^K we used a 4.5 μM solution in 1 mM HCl. Measurements of the three triblocks in the assembled state were performed as follows. For the acidic S^ECCS^E triblock a 1.5 μM solution in 10 mM HCl was prepared (final pH of 2.3), for the S^HCCS^H triblock a 1.5 μM solution in 20 mM phosphate buffer (final pH 7.9) was used, and measurements with the S^KCCS^K triblock were performed with a 4.5 μM solution in 20 mM NaOH (final pH 12.1). The solutions were left overnight to complete the self-assembly process before measuring the spectrum. The spectrum of a 1.5 μM solution of S^ECCS^E was recorded during the self-assembly process at different time intervals to examine the evolution of the secondary structure in time. Each measurement was performed in a 1 mm quartz cuvette.

Acknowledgment. The authors thank Aernout Martens and Monika Golinska for their help producing the triblock copolymers used in this research, and Adrie Westphal for his help on CD measurements. This research was funded by the Dutch Organization for Scientific Research (NWO).

REFERENCES AND NOTES

1. Shvetsov, A.; Galkin, V. E.; Orlova, A.; Phillips, M.; Bergeron, S. E.; Rubenstein, P. A.; Egelman, E. H.; Reisler, E. Actin Hydrophobic Loop 262−274 and Filament Nucleation and Elongation. *J. Mol. Biol.* **2008**, *375*, 793–801.
2. Guthold, M.; Liu, W.; Sparks, E. A.; Jawerth, L. M.; Peng, L.; Falvo, M.; Superfine, R.; Hantgan, R. R.; Lord, S. T. A Comparison of the Mechanical and Structural Properties of Fibrin Fibers with Other Protein Fibers. *Cell Biochem. Biophys.* **2007**, *49*, 165–181.
3. Goldsbury, C.; Baxa, U.; Simon, M. N.; Steven, A. C.; Engel, A.; Wall, J. S.; Aebi, U.; Muller, S. A. Amyloid Structure and Assembly: Insights from Scanning Transmission Electron Microscopy. *J. Struct. Biol.* **2011**, *173*, 1–13.
4. Labeit, S.; Ottenheijm, C. A. C.; Granzier, H. Nebulin, a Major Player in Muscle Health and Disease. *FASEB J.* **2011**, *25*, 822–829.
5. Arnaudov, L. N.; de Vries, R. Thermally Induced Fibrillar Aggregation of Hen Egg White Lysozyme. *Biophys. J.* **2005**, *88*, 515–526.

6. Arnaudov, L. N.; de Vries, R.; Ippel, H.; van Mierlo, C. P. M. Multiple Steps during the Formation of Beta-lactoglobulin Fibrils. *Biomacromolecules* **2003**, *4*, 1614–1622.
7. Pearce, F. G.; Mackintosh, S. H.; Gerrard, J. A. Formation of Amyloid-like Fibrils by Ovalbumin and Related Proteins under Conditions Relevant to Food Processing. *J. Agric. Food. Chem.* **2007**, *55*, 318–322.
8. Martens, A. A.; Portale, G.; Werten, M. W. T.; de Vries, R. J.; Eggink, G.; Stuart, M. A. C.; de Wolf, F. A. Triblock Protein Copolymers Forming Supramolecular Nanotapes and pH-Responsive Gels. *Macromolecules* **2009**, *42*, 1002–1009.
9. Smeenk, J. M.; Otten, M. B. J.; Thies, J.; Tirrell, D. A.; Stunnenberg, H. G.; van Hest, J. C. M. Controlled Assembly of Macromolecular Beta-sheet Fibrils. *Angew. Chem., Int. Ed.* **2005**, *44*, 1968–1971.
10. Smeenk, J. M.; Schon, P.; Otten, M. B. J.; Speller, S.; Stunnenberg, H. G.; van Hest, J. C. M. Fibril Formation by Triblock Copolymers of Silklike Beta-sheet Polypeptides and Poly(ethylene glycol). *Macromolecules* **2006**, *39*, 2989–2997.
11. Muller, M.; Krasnov, I.; Ogurreck, M.; Blankenburg, M.; Pazera, T.; Seydel, T. Wood and Silk: Hierarchically Structured Biomaterials Investigated in Situ with X-Ray and Neutron Scattering. *Adv. Eng. Mater.* **2011**, *13*, 767–772.
12. Nogueira, G. M.; de Moraes, M. A.; Rodas, A. C. D.; Higa, O. Z.; Beppu, M. M. Hydrogels from Silk Fibroin Metastable Solution: Formation and Characterization from a Biomaterial Perspective. *Mater. Sci. Eng. C* **2011**, *31*, 997–1001.
13. Byette, F.; Bouchard, F.; Pellerin, C.; Paquin, J.; Marcotte, I.; Mateescu, M. A. Cell-Culture Compatible Silk Fibroin Scaffolds Concomitantly Patterned by Freezing Conditions and Salt Concentration. *Polym. Bull.* **2011**, *67*, 159–175.
14. Tiyaboonchai, W.; Chomchalao, P.; Pongcharoen, S.; Sutheerawattananonda, M.; Sobhon, P. Preparation and Characterization of Blended Bombyx mori Silk Fibroin Scaffolds. *Fibers Polym.* **2011**, *12*, 324–333.
15. Ferguson, M. W. J.; Metcalfe, A. D. Tissue Engineering of Replacement Skin: The Crossroads of Biomaterials, Wound Healing, Embryonic Development, Stem Cells and Regeneration. *J. R. Soc. Interface* **2007**, *4*, 413–437.
16. Guille, M. M. G.; Helary, C.; Vigier, S.; Nassif, N. Dense Fibrillar Collagen Matrices for Tissue Repair. *Soft Matter* **2010**, *6*, 4963–4967.
17. Brown, R. A.; Wiseman, M.; Chuo, C. B.; Cheema, U.; Nazhat, S. N. Ultrarapid Engineering of Biomimetic Materials and Tissues: Fabrication of Nano- and Microstructures by Plastic Compression. *Adv. Funct. Mater.* **2005**, *15*, 1762–1770.
18. Lee, C. H.; Singla, A.; Lee, Y. Biomedical Applications of Collagen. *Int. J. Pharm.* **2001**, *221*, 1–22.
19. Schor, M.; Martens, A. A.; Dewolf, F. A.; Stuart, M. A. C.; Bolhuis, P. G. Prediction of Solvent Dependent Beta-Roll Formation of a Self-Assembling Silk-like Protein Domain. *Soft Matter* **2009**, *5*, 2658–2665.
20. Schor, M.; Ensing, B.; Bolhuis, P. G. A Simple Coarse-grained Model for Self-Assembling Silk-like Protein Fibers. *Faraday Discuss.* **2010**, *144*, 127–141.
21. Schor, M.; Bolhuis, P. G. The Self-Assembly Mechanism of Fibril-Forming Silk-Based Block Copolymers. *Phys. Chem. Chem. Phys.* **2011**, *13*, 10457–10467.
22. Wu, H. Correlations between the Rayleigh Ratio and the Wavelength for Toluene and Benzene. *Chem. Phys.* **2010**, *367*, 44–47.
23. Hadjichristidis, N.; Iatrou, H.; Pitsikalis, M.; Mays, J. Macromolecular Architectures by Living and Controlled/Living Polymerizations. *Prog. Polym. Sci.* **2006**, *31*, 1068–1132.
24. Martens, A. A. *Silk-Collagen-like Block Copolymers with Charged Blocks*; Wageningen University: Wageningen, 2008.
25. Li, F.; Martens, A. A.; Aslund, A.; Konradsson, P.; de Wolf, F. A.; Stuart, M. A. C.; Sudholter, E. J. R.; Marcelis, A. T. M.; Leermakers, F. A. M. Formation of Nanotapes by Co-Assembly of Triblock Peptide Copolymers and Polythiophenes in Aqueous Solution. *Soft Matter* **2009**, *5*, 1668–1673.